Collective Journal of Mechanical Engineering

Research Article

A Lamé Finite Element for the Initial Design of Rotating Discs

Abstract

Finite difference or conventional conforming finite element methods currently used for the analysis of rotating discs do not normally provide safe lower-bound predictions of the plastic burst speed. It is of potential concern when developing a disc geometry if later in the detailed design stage it is found to be structurally inadequate. This paper presents the development and illustrates the performance of an equilibrium finite element that provides safe lower-bound predictions of the plastic burst speed irrespective of mesh refinement. The element, which is termed the Lamé Finite Element, offers engineers a safe design methodology and, through dual analysis, the possibility to quantify the uncertainty in the burst speed prediction.

Keywords: Lamé Finite Element, Equilibrium Finite Element, Rotating Discs, Plastic Assessment, Burst Speed.

Introduction

In designing the rotors of high-speed turbomachinery, the engineer is primarily concerned with determining a disc geometry that has sufficient strength to withstand failure by bursting at the highest foreseen over-speed condition. The failure of a rotating disc by burst is an extremely serious event involving significant kinetic energy due to rotation being transferred to unconstrained disc fragments, typically a small number of disc sectors, and associated shrapnel which then act as projectiles. The avoidance by design of disc burst is a particular issue in aeroengines where the engine casing cannot economically be designed to constrain the post-failure projectiles.

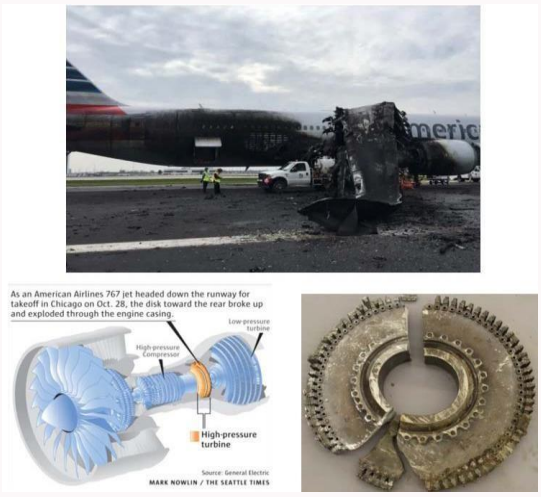

Figure 1: Images from an article in the Seattle Times [1].

Whilst, thankfully, rare, disc burst in aeroengines has occurred in commercial aircraft, typically during take-off when the engine is most highly loaded. In a rather clearly written article published on 4th November 2016 in the Seattle Times, Dominic Gates details one case of a disc burst in a GE aeroengine of a Boeing 767 as it was taking off from Chicago [1], and some of these images presented in this article are reproduced in Figure 1.

It is essential, therefore, that the engineer has robust analysis tools capable of predicting the burst of rotating discs of fairly arbitrary disc geometries with accuracy. It is also the case where the disc geometry is to be established through design-by-analysis that the tool is efficient so that a range of geometries may be considered with minimal computational effort.

By dint of the blades, the disc should be considered as a three-dimensional cyclic-symmetric model. It is traditional, however, to smear the loads of the blades over the entire periphery and adopt a two-dimensional axisymmetric continuum model. A further reduction of dimensionality from two to one is also generally acceptable where the disc exhibits symmetry about an axial plane and were

OPEN ACCESS

Authors:
*Angus Ramsay**

Affiliations:
PhD, FIMechE (Director), Ramsay Maunder Associates Limited, UK.

Corresponding Author:
Angus Ramsay, PhD, FIMechE (Director), Ramsay Maunder Associates Limited, UK.

Received Date: *11 Feb 2025*
Accepted Date: *24 Feb 2025*
Published Date: *19 Mar 2025*

Citation:
Angus Ramsay. A Lamé Finite Element for the Initial Design of Rotating Discs. Collect J Mech Eng. Vol 1 (1) 2025; ART0071.

the plane-stress constitutive relations are valid as is normally the case for rotating discs. In this manner the disc is represented as a line of variable thickness with only the radial and hoop stresses being considered. Such one-dimensional axisymmetric continuum models are quick to generate and analyses and, as such, are ideal for the initial design of rotating disc geometries. The features of the disc that are not captured accurately with such an idealization don't significantly influence the geometric design of the disc and can be dealt with at a later detailed design stage. Some of the modelling options and idealizations are illustrated in Figure 2.

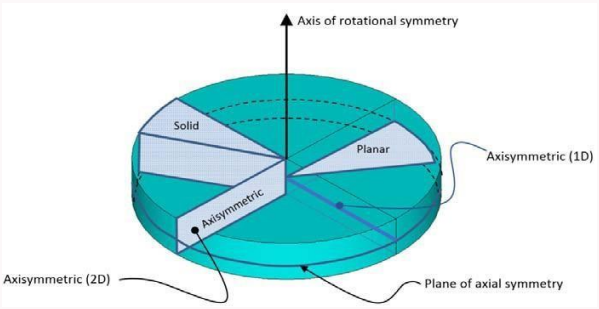

This image illustrates some of the options for modelling a rotating disc from three-dimensional solid continuum models and two-dimensional planar continuum models taking advantage of cyclic symmetry, through two and one-dimensional axisymmetric continuum models. The solid and planar models can take advantage of cyclic symmetry. The two-dimensional axisymmetric model may be reduced to half size by taking account of the plane of axial symmetry whereas the one-dimensional axisymmetric model assumes this to be the case.

Figure 2: Modelling options for a rotating disc [2].

There exist closed-form linear-elastic theoretical solutions for the one-dimensional idealization the simplest of which was presented by Lamé for discs with parallel sides, i.e., uniform thickness – see [3] for example. Theoretical solutions have also been established for more complex disc geometries, e.g., tapered geometries and the ubiquitous constant stress geometry. These have been presented in [4] and [5]. Although discs have been designed using such solutions, geometric features such as balancing or sealing rings often mean that these solutions cannot be used. In such cases the engineer resorts to numerical methods. In [5] the finite difference (FD) approach is presented and it is the experience of the author, who worked in the turbomachinery industry for a decade, that these approaches are still used.

As with all numerical methods, the FD approach produces an approximate solution whose convergent properties are not always clearly defined. The more modern finite element (FE) method is also approximate but can be shown, if the method is appropriately formulated, to converge to the theoretical solution with mesh refinement. For most finite element systems, in particular the large legacy systems, the formulation adopted is based on conforming displacements which leads, by definition, to compatible strains and is known as the conforming finite element (CFE) formulation. The displacement shape functions are generally polynomial and are, therefore, particularly unsuited to capturing the displacement variation in a rotating disc which, for the parallel sided disc, involves rational terms in the radial ordinate. As such, significant mesh refinement is required for such a CFE model to converge to the theoretical solution. The error in an unrefined CFE model manifests as a lack of equilibrium between the applied loads and the internal stress field and tends to lead to approximations that produce unsafe upper-bound predictions of quantities such as the burst speed. Thus, in order to achieve a result that can reliably used in design, the engineer needs to undertake a process of solution verification [6], which enables extrapolation to an estimate of the theoretical solution. Unfortunately, in the majority of commercial FE systems solution verification is a manual process requiring not inconsiderable effort from the engineer which tends to detract from the task in hand, i.e., the design of a structurally sound disc geometry.

Through a belief in common with his colleagues that the practicing engineer is better served using an equilibrium finite element (EFE) formulation, the author has devoted a significant part of his career to the research, development and application of such models. With an EFE formulation strong equilibrium is guaranteed ensuring that predictions of the burst speed converge from below the theoretical solution. In this manner the solution from even the crudest meshes are safe and the engineer can concentrate on the disc design comforted by the knowledge that even without formal solution verification, the burst speed predicted by the model will lie on the safe side of truth.

In this paper the Lame solution for parallel-sides rotating discs with a plane-stress constitutive relation is used to construct a finite element stiffness matrix and load vector. The resulting element is one where both strain/displacement compatibility and stress/load equilibrium are satisfied exactly and, in this sense, it is a Trefftz finite element (TFE) formulation [7]. These elements can be assembled in the usual manner to provide models that represent the true disc geometry in a piecewise uniform fashion.

In contrast to a CFE model, which requires considerable mesh refinement to recover a reasonable approximation to the linear-elastic solutions governed by the Lamé equations, the TFE model will recover the solution with a single element. For this reason, the author has called this element the Lamé finite element (LFE).

Like rotating discs, pressure vessels are another safety critical component where LFE would provide a sensible and safe alternative to conventional methods. Pressure vessels can burst in a ferocious nature particularly when containing compressible gases – see Figure 3 which presents an image taken from [8].

Figure 3: Image of burst pressure vessels [8].

Much research has been undertaken into the advantages of pressure vessels formed of compound rings and there are many published examples where the Lamé equations are laboriously written out for each ring and then coupled with the appropriate continuity conditions. This approach probably comes from strength of material texts where it is often presented as a method for such components – see for example [3]. A far tidier approach would be to adopt a mesh of LFEs. Although not considered in this paper, the load vector for thermal body loads is simply determined and the contact condition between adjacent rings can be handled efficiently using gap elements and an iterative analysis. The first example shown in this paper illustrates the performance of an LFE model and compares this to that of CFE models for a pressurized pipe or vessel.

Plasticity is considered in the examples presented in this paper. In determining the plastic limit load the material is often idealized as an elastic, perfectly-plastic material model and this idealization will be used in this paper. Strain-hardening could be included and would certainly be included at the detailed design stage. However, for the initial design of disc geometry ignoring strengthening likely to be achieved through strain-hardening is considered a reasonable conservative approach.

In modelling the plastic behavior of the disc material as the speed increases beyond that which causes first yield, a number of numerical approaches may be adopted. As the plastic limit load or burst speed is unique then this measure should be independent of the approach used. The common approach used in commercial FE systems is the incremental approach [9]. Here the load is applied incrementally based on a linearized extrapolation of the material state at the start of the iteration. After each increment an iterative approach is required to bring the solution back onto the correct material state.

An alternative approach that exploits the strong equilibrium from EFE models is that of lower-bound limit analysis. An example of this approach for plate elements is shown in [10]. In this approach a solution from a linear-elastic EFE model is used as a particular solution. To this solution is added a set of self-balancing or hyperstatic stress fields the amplitudes of which are determined in a mathematical program so as to maximize the load factor whilst respecting the yield constraints. This approach has been successfully implemented for the LFE model.

A third approaches the elastic compensation method (ECM) [11]. This is a very simple iterative approach that is easily implemented in software. It is rather flexible in terms of the yield criterion adopted and has been used to produce the plastic solutions presented in this paper. It is worth noting with regard to the material idealization used in this paper that no strain limit has been accounted for in the solutions. The assumption made is that the material has sufficient ductility to allow the plastic solution to fully develop. Whilst the materials used for real discs is usually ductile, this property will have some limit and will certainly need to be formally checked at the detailed design stage.

The two yield criteria generally adopted for ductile metals are the Tresca and the von Mises criteria. The work of Taylor & Quinney [12], has demonstrated that the von Mises criterion provides a more accurate representation of yield than the Tresca criterion – see Figure 4. The simplicity of the Tresca criterion, which is a conservative linearization of the von Mises criterion, means that it is often used in the development of theoretical solutions – see for example [13].

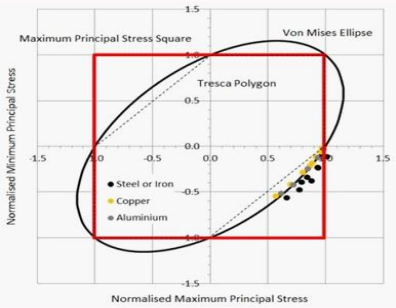

Figure 4: Reproduction of results from Taylor & Quinney [12].

It is the case, as seen in Example 1, that even for a uniform thickness geometry where the elastic solution is exact, mesh refinement is required to obtain an accurate prediction of the corresponding plastic solution. The iterations required by the ECM are based on linear elastic solutions and so the solution at any stage of mesh refinement and plastic iteration is an equilibrium solution and offers a lower-bound estimate of the burst load.

Following Example 1 a section is introduced to illustrate how the piecewise uniform thickness LFE model provides predictable lower-bound solutions for disc geometries that are not parallel-sided but where the thickness decreases monotonically with increasing radius. This feature is further demonstrated in Example 2 which shows how an LFE model can accurately capture the solution for the well-known case of the uniform strength disc.

In Example 3 the analysis of a real rotor with blade loads is considered. Results from two elastic finite difference (FD) methods have been published and the performance of an LFE model is compared with these results.

The practical advantages of the LFE method over the FD of CFE approaches means that a safe and reliable tool could be developed for the design-by-analysis of rotating discs. An example of this technique is presented in Example 4 where the geometry of the disc is modelled using a cubic Bezier curve. Two geometric variables (position of the Bezier control points) are considered and design curves are produced and overlaid on a contour plot of disc mass. Although relatively simply, this example demonstrates the relative ease with which a design-by-analysis tool can be developed. It should be noted that this sort of tool could be developed into a real-time analysis tool where the control points are moved around through user interaction with the mouse. Even though to achieve full convergence in the earlier examples extremely refined LFE meshes have been used, with reasonable computing power these models take only a few fractions of a second to complete.

In the discussion section consideration is given to the performance of burst predictions based on elastic rather than plastic analysis. Criteria such as the Robinson Burst Criteria define the speed of burst as that when the average elastic hoop stress reaches the ultimate strength of the material. This criterion gives an exact prediction for uniform thickness discs but is approximate and unsafe for other non-uniform disc geometries. It is also the case that hoop burst is not the only form that might occur in a rotating disc. Whereas hoop burst essentially requires the entire disc to reach a plastic state, a form of failure called radial burst can and does occur in discs geometries where the web between hub and rim is essentially parallel sided. The disc considered in Example 3 has the sort of geometry where radial burst occurs. At a given radius the radial stress reaches yield which, at least for the Tresca yield criterion, indicates failure around an annular ring of the disc. Again, the strong equilibrium achieved with an LFE model ensures that this mode of failure is accurately captured.

Given that CFE and LFE models provide upper and lower bounds on the exact solution, the idea of dual analysis to quantify the uncertainty in a particular solution is discussed. In this work it has been observed that the stiffness matrix for the CFE element when using reduced integration is identical to that of the LFE element. This means that with suitable modified post-processing of the CFE results the same solution obtained with an LFE model can be obtained at minimal computation cost and without the necessity for reanalysis of the model.

In the final section of this paper, conclusions are drawn as to the utility of the LFE method for the practical initial design of rotating discs and ideas for further developments are expressed.

The Lamé Equations

In this section the essential steps in the derivation of the Lamé equations are stated. The complete derivation can be found in many standard and advanced texts, for example, see [14]. The geometrical parameters involved in the representation of a rotating disc and the boundary terms are illustrated in Figure 5.

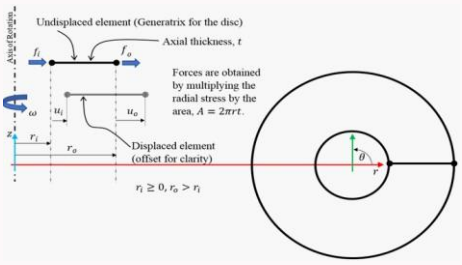

Figure 5: Geometric definition and boundary terms for an LFE.

In this paper we consider a uniform thickness axisymmetric body defined in a cylindrical coordinate system, r, θ. Boundary loading will be considered along with body loading due to a constant angular velocity, ω. For the isotropic materials considered in this paper, the elastic properties of the material are defined by the elastic modulus, E, and Poisson's ratio, ν, with the mass density of the material denoted by ρ. In the absence of torque and angular acceleration there are no shear stresses or strains and the two stress components of interest are the radial stress, σ_r and the circumferential or hoop stress, σ_h which have corresponding strains ε_r and ε_h respectively, these then being principal values. The equations of equilibrium, constitution and compatibility for this axisymmetric problem are given in Eq. (1).

$$\sigma_h - \sigma_r - r\frac{d\sigma_r}{dr} = \rho r^2\omega^2 \qquad \text{Equilibrium} \qquad (1a)$$

$$\begin{Bmatrix}\varepsilon_r\\ \varepsilon_h\end{Bmatrix} = \frac{1}{E}\begin{bmatrix}1 & -\nu\\ -\nu & 1\end{bmatrix}\begin{Bmatrix}\sigma_r\\ \sigma_h\end{Bmatrix} \qquad \text{Constitutive (plane-stress)} \qquad (1b)$$

$$\varepsilon_r = \varepsilon_h + r\frac{d\varepsilon_h}{dr} \qquad \text{Compatibility} \qquad (1c)$$

Although a plane-strain constitutive relationship between stresses and strains may be appropriate for rotating components with large axial thickness, e.g., a shaft, the plane-stress relation is universally considered appropriate for rotating discs which have relatively thin axial dimensions.

Combining the three equations, Eq. (1), and recognizing the appropriate strain displacement relations leads to the second-order differential equation given in Eq. (2) which can be solved for the radial displacement, u.

$$\frac{d^2u}{dr^2} + \frac{1}{r}\cdot\frac{du}{dr} - \frac{u}{r^2} + (1-\nu^2)\cdot\frac{\rho\omega^2 r}{E} = 0 \qquad (2)$$

The Lamé equations, Eq. (3), give a solution to this differential equation in terms of the two Lamé coefficients, a and b. These coefficients are determined from the boundary conditions for the problem.

$$\sigma_r = a - \frac{b}{r^2} - (3+\nu)\frac{\rho\omega^2 r^2}{8} \qquad (3a)$$

$$\sigma_h = a + \frac{b}{r^2} - (1+3\nu)\frac{\rho\omega^2 r^2}{8} \qquad (3b)$$

$$u = \frac{r}{E}(\sigma_h - \nu\sigma_r) \qquad (3c)$$

Development of the Element Stiffness Equations

For a force-driven problem, with radial boundary forces, f_i and f_o, at the inner and outer radii, r_i and r_o, the Laméco efficient may be determined from Eq. (4), where $\boldsymbol{E}$ transforms boundary forces into corresponding internal stresses and is thus termed the Equilibrium Matrix.

$$\begin{Bmatrix}a\\ b\end{Bmatrix} = \boldsymbol{E}\begin{Bmatrix}f_i\\ f_o\end{Bmatrix}$$

$$\boldsymbol{E} = \frac{1}{2\pi t(r_o^2 - r_i^2)}\begin{bmatrix}r_i & r_o\\ r_i r_o^2 & r_i^2 r_o\end{bmatrix} \qquad (4)$$

Whilst the matrix $\boldsymbol{E}$ is singular for an element with the inner node on the axis of rotation, i.e., $r_i = 0$, the inverse of this matrix, $\boldsymbol{E^{-1}}$, may be written explicitly as shown in Eq. (5).

$$\boldsymbol{E^{-1}} = 2\pi t\begin{bmatrix}-r_i & 1/r_i\\ r_o & -1/r_o\end{bmatrix} \qquad (5)$$

A similar expression can be written in terms of radial boundary displacements, u_i and u_o, for displacement driven problems as shown in Eq. (6), where $\boldsymbol{C}$ transforms boundary displacements into corresponding internal strains and is thus termed the Compatibility Matrix

$$\begin{Bmatrix}a\\ b\end{Bmatrix} = \boldsymbol{C}\begin{Bmatrix}u_i\\ u_o\end{Bmatrix}$$

$$\boldsymbol{C} = \frac{E}{r_o^2 - r_i^2}\begin{bmatrix}r_i/(\nu-1) & -r_o/(\nu-1)\\ r_i r_o^2/(\nu+1) & -r_i^2 r_o/(\nu+1)\end{bmatrix} \qquad (6)$$

In the absence of body and thermal loads, Eq. (4) determines the Lamé coefficients for a force driven problem whereas Eq. (6) does so for a displacement driven problem. Whilst the vast majority of Lame problems are force

driven, one can conceive of other problems which are displacement driven or mixed problems. It is necessary, therefore, to be able to identify a solution of the Lame equations that copes with the full range of possible boundary conditions and such a general solution can be obtained by equating Eq. (4) to Eq. (6) as shown in Eq. (7). In this manner the Lamé coefficients are eliminated leading to two equations expressed in terms of the two boundary forces and displacements which may be solved for arbitrary boundary condition specifications.

$$\boldsymbol{Cu} = \boldsymbol{Ef} \tag{7}$$

A standard stiffness formulation with the stiffness matrix $\boldsymbol{K}$ can be derived from Eq. (7) as shown in Eq. (8).

$$\boldsymbol{E^{-1}} = \boldsymbol{Cu} = \boldsymbol{f} = \boldsymbol{Ku}$$
$$\boldsymbol{K} = \frac{2E\pi t}{(1-\nu^2)(r_o^2 - r_i^2)} \begin{bmatrix} (1+\nu)r_i^2 + (1-\nu)r_0^2 & -2r_i r_o \\ -2r_i r_o & (1-\nu)r_i^2 + (1+\nu)r_0^2 \end{bmatrix} \tag{8}$$

One of the properties of an element stiffness matrix is, according to the Maxwell-Betti reciprocal theorem, that it should be symmetric, and this property is seen observed for the LFE. Since there are no rigid-body modes of displacement associated with this element, the stiffness matrix is non-singular for $r_o > r_i$, and could be inverted into a flexibility matrix if so desired.

Body Loading

This form of loading was neglected in the development of the stiffness equations in order to concentrate the reader's mind on the direct formulation presented. It is, however, simply included by adding the appropriate term to the right-hand side of the stiffness equations. If body loading is included then the equilibrium equations of Eq. (4) expands to the form shown in Eq. (9).

$$\begin{Bmatrix} a \\ b \end{Bmatrix} = \boldsymbol{Ef} + \boldsymbol{b_f}$$
$$\boldsymbol{b_f} = (3+\nu)\frac{\rho\omega^2}{8}\begin{Bmatrix} r_i^2 + r_o^2 \\ r_i^2 r_o^2 \end{Bmatrix} \tag{9}$$

Alternatively, the compatibility formulation of the system of equations is as shown in Eq. (10).

$$\begin{Bmatrix} a \\ b \end{Bmatrix} = \boldsymbol{Cu} + \boldsymbol{b_u}$$

Alternatively, the compatibility formulation of the system of equations is as shown in Eq. (10).

$$\begin{Bmatrix} a \\ b \end{Bmatrix} = \boldsymbol{Cu} + \boldsymbol{b_u}$$

$$\boldsymbol{b_u} = \frac{\rho\omega^2}{8}\begin{Bmatrix} (\nu+1)(r_i^2 + r_o^2) \\ (\nu-1)r_i^2 r_o^2 \end{Bmatrix} \tag{10}$$

As already shown, equating Eq. (9) and Eq. (10) eliminates the Lamé coefficients and pre-multiplying by $\boldsymbol{E^{-1}}$ leads to Eq. (11) which are the stiffness equations including the full set of boundary and body loading.

$$\boldsymbol{Ku} = \boldsymbol{f} + \boldsymbol{b}$$
$$\boldsymbol{b} = \boldsymbol{E^{-1}}\{\boldsymbol{b_f} - \boldsymbol{b_u}\} \tag{11}$$

The matrix $\boldsymbol{E}$ is singular when $r_i = 0$ but this singularity can be bypassed by expanding the expressions in Eq. (11) symbolically as shown in Eq. (12).

$$\boldsymbol{b} = \frac{\rho\omega^2\pi t}{2}\begin{Bmatrix} r_i r_o^2 - r_i^3 \\ r_o^3 - r_i^2 r_o \end{Bmatrix} \tag{12}$$

Post-Processing & Results

The stiffness equations for a single LFE element are assembled in the usual manner to form the structural stiffness equations for the disc, the solution to which comprises the nodal displacements. The nodal forces that hold each element in equilibrium with respect to the applied loading are simply recovered using the nodal displacements in the stiffness equations for the element and the internal stresses and displacements can be recovered using Eq. (3) once the Lamé Coefficients for an element have been evaluated using either Eq. (9) or Eq. (10).

The radial, σ_r, and hoop stress, σ_h are principal stresses. It is common, for the sort of ductile metals used for rotors, to adopt the von Mises yield criterion as the failure criterion. For this yield criterion the so-called 'equivalent stress', S_E, is given by Eq. (13c) and the maximum principal stress and Tresca criterion which will also enter into the discussion are expressed in Eq. (13a) and Eq. (13b) respectively.

Yield Criterion	Expression	
Maximum Principal Stress	$\max\{\text{abs}(\sigma_r), abs(\sigma_h)\}$	(13a)
Tresca	$\max\{\text{abs}(\sigma_r - \sigma_h), \text{abs}(\sigma_r), abs(\sigma_h)\}$	(13b)
Von Mises	$(\sigma_r^2 + \sigma_h^2 - \sigma_r\sigma_h)^{1/2}$	(13c)

A linear-elastic solution is only valid if the maximum value of the equivalent stress in the rotor is less than or equal to the yield stress, S_Y, this usually being determined from a uniaxial tensile test. The maximum equivalent stress, $\hat{S}_E$, occurs at a point termed the 'critical' point or radius. When discussing and plotting yield diagrams it is common to work in terms of normalized principal and equivalent stresses. The normalization involves dividing by the yield stress and normalized quantities are indicated with the tilde, so, for example, the normalized equivalent stress at a particular point would be $\tilde{S}_E = S_E/S_Y$. The maximum normalized equivalent stress is given the symbol $\dot{S}_E$.

An engineer designing a rotor would typically need to ensure that the maximum equivalent stress at the operating or design speed, ω_d, is below some prescribed design stress. Note that the analysis is generally undertaken at the design speed. At the detailed design stage, the design stress will typically be based on considerations of fatigue/creep failure and is likely to be a fraction of the yield stress for the material.

At the initial design stage, however, the disc will generally be designed based on the plastic burst speed, ω_p , which is the output of a plastic analysis. A non-dimensional plastic load factor, λ_p, may be defined as given in Eq. (14).

$$\lambda_p = \left(\frac{\omega_p}{\omega_d}\right)^2 \tag{14}$$

The elastic limit speed is often also of interest, ω_e as the speed at which first yield occurs and the corresponding elastic load factor is defined in Eq. (15) where the manner in which ω_e is calculated based on the elastic stress is shown.

$$\lambda_e = \frac{S_Y}{\hat{S}_E} = \frac{1}{\dot{S}_E} = \left(\frac{\omega_e}{\omega_d}\right)^2 \tag{15}$$

Despite the seemingly counter-intuitive idea that stress measures from an elastic analysis might be helpful in the prediction of plastic burst, such metrics have and are still used in the early design stages of a rotating disc. These stress metrics are shown in Eq. (16).

$\bar{\sigma}_h = \frac{1}{A}\int \sigma_h \, dA$ Average (elastic) hoop stress (AHS) (16a)

$\hat{\sigma}_r = \max(\sigma_r)$ Maximum (elastic) radial stress (MRS) (16b)

The predicted burst speed associated with the stress metrics given in Eq. (16) are provided in Eq. (17).

$$\omega_{AHS} = \omega_d\sqrt{\frac{S_Y}{\bar{\sigma}_h}} \tag{17a}$$

$$\omega_{MRS} = \omega_d\sqrt{\frac{S_Y}{\hat{\sigma}_r}} \tag{17b}$$

In addition to point displacements and stresses, there are some additional model metrics that are useful when it comes to the design of rotors. Obvious candidates here are the mass and inertia of the rotor as one of these will tend to be the objective function in a design scenario. Another useful measure is the utilization, U. This is a measure of how well the capacity of the rotor is being used and lies in the range $0 \le U \le 1$. It can be considered as a pointwise quantity defined as S_E/S_Y or, perhaps more usefully, as an average value for the entire rotor as shown in Eq. (18) where A is the area of the rotor generatrix.

$$U = \frac{1}{A}\int \frac{S_E}{S_Y} dA \tag{18}$$

This quantity can be evaluated for the elastic and plastic limit solutions and will be identified with the appropriate subscripts, i.e., U_e for the average utilization at the elastic limit and U_p for that at the plastic limit speed. For the so-called 'uniform strength' disc geometry, the elastic and plastic utilizations are unity, i.e., the full available capacity of the rotor is being utilized – see Example 2. For most rotors, however, the average elastic utilization will be less than unity, and sometimes considerably less than unity. Plastic redistribution will generally increase the average utilization and depending on whether or not the full rotor can be utilized in this manner the average plastic utilization can often reach unity even when the elastic value might be significantly less than unity.

Example 1: Pressurized Thick Cylinder

A thick cylinder shown is defined with $r_i = 0.1m$ and $r_o = 1m$. The internal and external pressures, are, respectively, p_i and p_o. Two load cases are considered as defined by the Lamé coefficients a=100kPa, b=0,

(LC1), and a=0, b=100kN, (LC2). Using an elastic modulus of 200GPa, Poisson's ratio of 0.3, an axial thickness of 0.01m and a plane-stress constitutive relationship, the radial and hoop stresses are as presented in Figure 6.

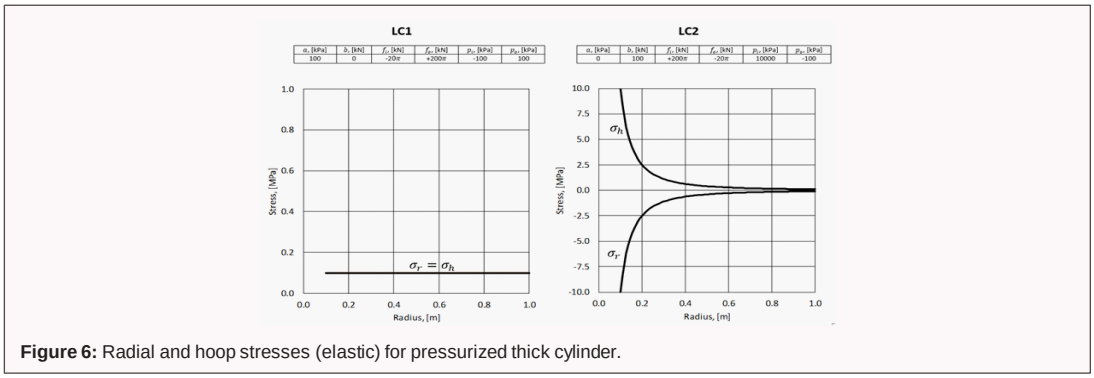

Figure 6: Radial and hoop stresses (elastic) for pressurized thick cylinder.

For LC2 we see quite clearly one of the properties of the Lamé equations in the absence of mechanical or thermal body loading, namely, that the sum of the radial and hoop stresses at any point is equal to twice the first Lamé coefficient, i.e., $\sigma_r + \sigma_h = 2a$, where, in this case, $a = 0$.

Using the axisymmetric shell from a commercial CFE system and with the bending part of the element switched off, the exact solution for LC1 is recovered with a single lower or higher order CFE element. This is not surprising since the exact stresses are constant with respect to radius. For LC2, on the other hand, the CFE element which even with the higher order element only has linear stress capability, struggles to simulate the $1/r^2$ term present for both the stresses in the closed-form solution as shown in Figure 7. For both lower and higher order elements a significant number of elements are required before the asymptotic region of uniform convergence rate is reached. Both elements underpredict the exact stress and by significant amounts for coarse meshes and this could lead to a potentially unsafe design were the engineer not to detect the poor quality of the result.

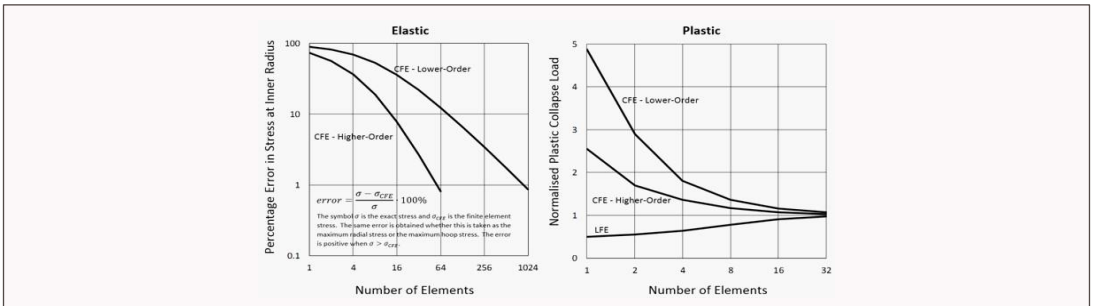

Figure 7: Convergence of elastic stress and plastic load factor for LC2.

The LFE recovers the exact elastic solution for both load cases and provides a safe and accurate prediction of the plastic collapse load.

Bounded Nature of the LFE Stresses

The LFE satisfies all the governing equations internally and both equilibrium and compatibility between elements. The element is exact provided the thickness of the rotor is uniform. If the thickness is not uniform then a mesh of uniform thickness LFE elements may be used with each element taking on the average thickness of the actual geometry at the two ends of the element. The LFE solution remains exact for the idealized, elementwise or piecewise uniform thickness geometry but is only an approximation to that for the exact geometry and mesh refinement will be required to converge towards the exact solution.

It is also the case that even if the actual geometry has uniform thickness, then the plastic solution obtained using the ECM will generally be approximate and require mesh refinement to converge towards the exact solution. For this case, where the actual geometry has uniform or even piecewise uniform thickness, the elastic solutions are exact and, provided the equivalent stresses remain within the yield criterion then the lower-bound theorem of plasticity can be invoked. The plastic limit load will then be a safe, lower-bound prediction of the exact value. This behavior was observed in Example 1 where it was seen in Figure 6 that the plastic collapse load converged towards the true value from below.

It is the case then that for a typical rotor, which will have an arbitrary but non-uniform thickness variation, a mesh of LFEs will be required to capture the true solution. If the mesh is not adequate then the elastic solution will be exact and the plastic solution safe but only for the elementwise uniform thickness idealization. In general, this

approximate solution might not be a bound on the solution for the exact geometry. However, for rotor geometries which are normally convergent, i.e., the thickness decreasing with increasing radius, it may be argued for the idealized geometry, which attracts greater centrifugal loading than the exact geometry, that the stresses will normally be greater than those for the actual geometry and, as a result, the bounded nature of the idealized LFE solution holds.

A convergent, tapered geometry is shown in blue in Figure 8. The figure also shows the idealization of this geometry with a single LFE with uniform thickness equal to the mean thickness of the tapered geometry.

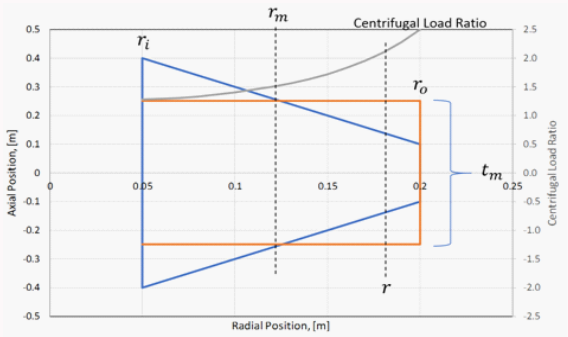

Figure 8: Centrifugal load ratio for a single LFE.

If it can be shown that the centrifugal loading at all radial positions is greater for the idealized uniform thickness geometry than for the actual tapered geometry then it is reasonable to expect the same for the stresses. From the figure it is evident that the centrifugal loading at radius, r, due to the material between this radius and the outer radius, r_o, is going to be different for the idealized geometry than for the tapered geometry. For $r > r_m$ the centrifugal force for the idealized geometry, C_i, will certainly be greater than that for the actual geometry, C, i.e., the centrifugal load ratio $C_i/C >$ unity. As the radius is moved below the mean radius towards the inner radius then the ratio will decrease. However, even though the difference in areas in the generator plane between the idealized and actual geometries are identical either side of the mean radius, the mass and centrifugal load developed by the area to the left of the mean radius are smaller than those to the right of the mean radius. As such, the centrifugal load ratio remains greater than unity at the inner radius. This means that for all radial positions in the uniform thickness LFE, the body loading is greater than that for the actual convergently tapered geometry. The centrifugal load ratio has been included in the figure and demonstrates the form of behavior described.

Although the previous analysis would indicate that, because the centrifugal load ratio is greater than unity over the complete radial dimension of an LFE, this alone does not guarantee the LFE stresses will be greater than those for the actual geometry. What is missing is the influence of the radial stress resultants applied to the ends of the elements.

For the LFE model, the actual radial force is applied to the ends of the model, e.g. due to the blade load, so that the radial stress resultants are correct. Clearly, though, the radial stress will not be correct as the axial thickness for the LFE is different than the true value. Thus, one would expect that the radial stress at the outer radius of an LFE will be less than the true value whereas the same stress at the inner radius of the element will be greater than the true value. This idea can be demonstrated through an example.

Example 2: Uniform Strength Rotor

The case considered here is that of a uniform strength rotor the thickness distribution for which is given in Eq. (19), [14].

$$t = t_o e^{\frac{-\rho\omega^2 r^2}{2\sigma}} \qquad (19)$$

The values for the quantities defined in Eq. (19) used for this example are given in Table 1.

Table 1: Parameters defining uniform strength rotor

Quantity	Value
r_i, [m]	0.0
r_o, [m]	0.2
t_o, [m]	0.2
ρ, [kg/m³]	7800
ω, [rad/sec]	2000
σ, [MPa]	275

Although with the uniform strength disc the thickness profile is now curved, the degree of curvature is not significant so that whilst not strictly true, one may adopt the same argument used for the tapered geometry particularly as the LFE mesh is refined.

LFE solutions will be considered for meshes of 1, 2, and 4 LFE elements. The radial force stress resultants for the three meshes considered are compared, in Figure 9, with those for a mesh of 256 LFEs – this being very close to the theoretical solution for the problem.

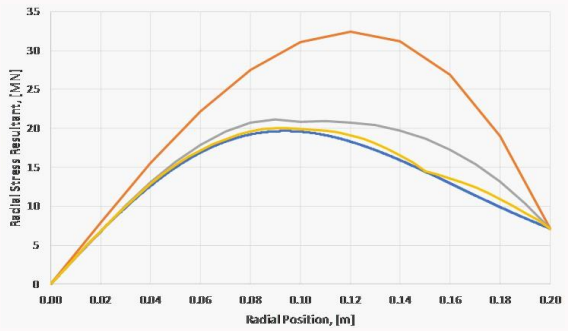

Figure 9: Radial stress resultants for LFE meshes.

The stress resultants at the ends of the model where the static boundary conditions are applied are exact for all LFE meshes. Between the ends the stress resultants for LFE meshes are greater than the true values with minimum difference being observed at the internal nodes.

Thus, one would expect that the LFE stresses exceed those for the true geometry. This, however, is not the case as, at the outer radius of an element, the thickness is greater than the actual value. As such, the predicted radial stress will be less than the true value. At the inner radius of the element the opposite is true and the radial stress at this position will be greater than the true value. This point is demonstrated in Figure 10 where the equivalent stress is plotted as a function of radius for the meshes considered.

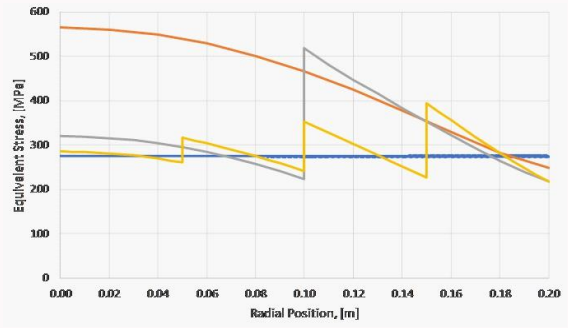

Figure 10: Equivalent stresses for LFE meshes.

Although the stresses from the LFE model do go below the theoretical solution particularly at the outer radius of each LFE, the maximum stresses for a given mesh, as indicated in the figure with red circles, remain above the theoretical value.

On the basis of the above analysis, it is reasonable to assume that for convergent rotor geometries that the maximum elastic stress is greater than the theoretical value and, therefore, leads to a safe bound for the elastic load factor. The convergence of the elastic load factor with uniform mesh refinement is shown in Figure 11. The rate of convergence for selected segments has been added to the figure with refinement appearing to lead to a unit convergence rate.

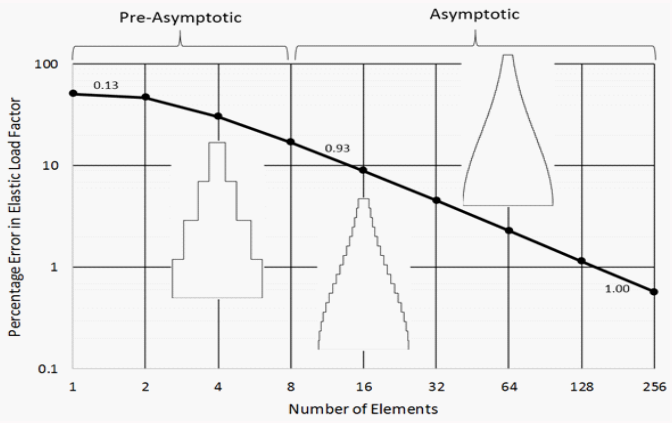

Figure 11: Convergence of the error in elastic load factor for LFE meshes.

Example 3: Analysis of a Rotor

The example chosen here comes from Chapter 12 of [5] which deals with numerical methods for discs of arbitrary profiles. The disc geometry, material properties and loading are provided in Figure 12.

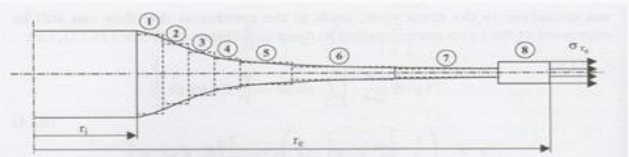

Fig. 8.1 Variable profile disk and breakdown into eight partial disks having constant thickness (projection lines are omitted)

Table 8.1 Geometry of constant-thickness partial disks, operating conditions and material properties

$E = 2.1 \cdot 10^5$ GPa	$\gamma = 7{,}800$ kg/m^3
$\nu = 0.30$	$\omega = 314$ rad/s
$r_e = 0.5$ m	$\sigma_{re} = 10$ MPa
$r_i = 0.1$ m	$\sigma_{ri} = 0$

Partial disk	Inner radius (m)	Outer radius (m)	Thickness (m)
1	0.100	0.125	0.100
2	0.125	0.150	0.070
3	0.150	0.175	0.050
4	0.175	0.200	0.035
5	0.200	0.250	0.025
6	0.250	0.350	0.015
7	0.350	0.450	0.010
8	0.450	0.500	0.025

Figure 12: Rotor problem considered for analysis [5].

Two FD methods are presented in the text, these are the Timoshenko-Grammel Method, [15,16], and the Manson Method, [17]. Stresses for both methods are presented for the piecewise uniform or stepped thickness idealisation of the disc in Figure 13.

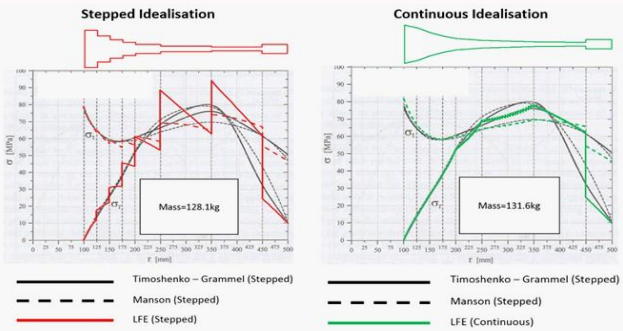

Figure 13: Principal stresses from LFE compared with other numerical approaches [5].

The stresses from the numerical methods presented in [5], differ by about 7% in the regions where the stresses are maximum depending on the method adopted. It is clear that they do not satisfy equilibrium exactly as this requires a step change in the radial stress across the interfaces of the stepped geometry. The exact elastic stresses obtained using LFE have been superimposed on the figure. It is interesting to note that Manson's FD method agrees well with the LFE stresses if average values are taken across the stepped interfaces.

In addition to the stepped idealization, a continuous idealization has also been considered using LFE. No results are available for this idealization from the FD methods and so the LFE results for the continuous idealization are overlaid on the FD results for the stepped idealization. The LFE model adopts a mesh of 20 uniform thickness LFEs per segment, i.e., 160 elements in total.

The radial stress for the continuous idealization of LFE between r=250 and 350mm appears flattened when compared to the results of Manson or Timoshenko-Grammel. However, the result was checked using CFE and found to be correct. The flattening is therefore taken to be an artefact of the way in which the stepped idealization was crudely converted to a continuous one, i.e., the curve is only C_0 continuous.

The equivalent stress as a function of radius for both the elastic and the plastic limit loads are shown in Figure 14 together with the corresponding load factors and utilizations.

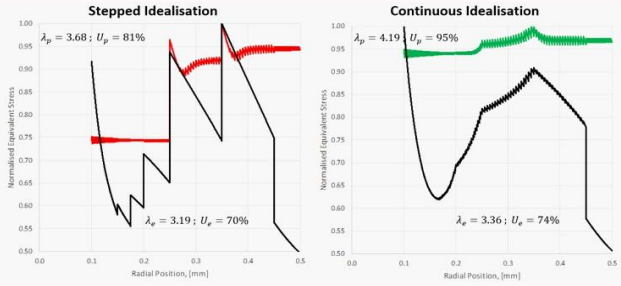

Figure 14: Equivalent stresses, elastic and plastic, for the rotor.

The continuous idealization of the rotor moves the maximum stress from a radius of about 0.35 to the inner radius and pushes up the elastic load factor in the process. The continuous idealization is also better able to redistribute the stresses than the stepped geometry as indicated by the increased plastic utilization and the enhanced burst speed which increases from 602 to 643 rad/sec – c.f., Eq. (17).

The normalized elastic and plastic principal stresses are shown in the von Mises yield surface in Figure 15. The curves plot the equivalent stresses from the inner radius to the outer radius of the rotor where the inner radius can be easily identified as the radial stress is zero. The black curves are the elastic solutions and the colored curves the plastic solutions. All curves have a critical point where the equivalent stress just touches the yield surface, the stress at all other radii lying within the surface.

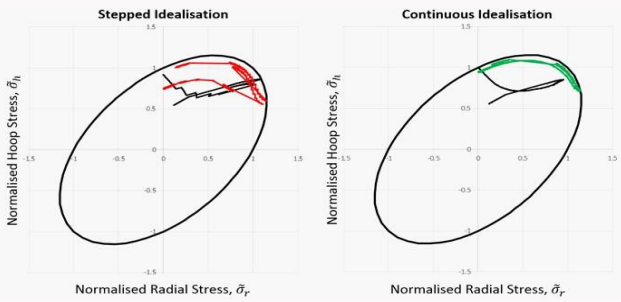

Figure 15: Principal stresses in the von Mises yield surface.

Given that actual rotor has a continuous and smooth thickness profile then the results for the continuous idealization produced using LFEs is likely to be closer to the solution for the actual rotor than that of the stepped idealization. It is both interesting and curious that the stresses from the two FD methods presented in [5], which are apparently based on the stepped idealization, are, for the most part, in good agreement with the LFE results for the continuous idealization.

Example 4: Design of a Rotor

Whereas analysis of a rotor requires the engineer to determine the structural metrics of interest for a predetermined rotor geometry, design involves finding feasible rotor geometries for which the structural metrics

satisfy the required performance criteria. There will generally be a range of such feasible rotor geometries and selection from these might be made on the basis of minimum cost which for a rotor would typically be equivalent to minimum mass. This then defines a formal constrained optimization process.

In the initial design stage, the engineer will be interested in determining a rotor geometry which has sufficient fatigue life for the duty of the rotor and sufficient burst margin for the machine. Fatigue life and burst margin are quantified using the maximum elastic stress, i.e., the elastic load factor, and the plastic load factor. Both these quantities are determined in a conservative manner for LFE models making this approach ideally suited for the initial design of rotors. There will, of course, need to be further detailed design work undertaken on the rotor to deal with a range of additional matters such as stress concentrations around the hub/web the rim/web interfaces and any holes incorporated in the rotor, addition of rings for sealing and balancing purposes and, importantly for high-speed turbomachinery, dynamic considerations, e.g., vibration resonances. These are generally considerations dealt with once an initial structurally feasible design has been established and are not considered further in this paper.

A design program for the rotor would require, primarily, a method of idealizing the geometry in terms of geometric variables. For a given set of values for these variables, a sensibly refined LFE model could then be used to establish the elastic and plastic load factors together with the mass of the rotor. This could then be used as the calculation engine for a constrained optimization algorithm to seek out the particular set of geometric variables that minimizes the mass of the rotor. In this example such an algorithm is not used and, instead, the design process will be presented as an exploration of the design space which is then characterized using contours of load factor superimposed on contours of rotor mass.

A rotor similar to that analyzed in the previous section of this paper will be used as a candidate for design optimization. The rotor geometry will be defined using a single cubic Bezier curve constrained to have two geometric variables as shown in Figure 16 where the rotor design problem is defined.

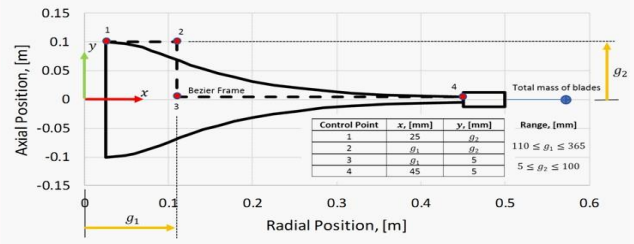

Figure 16: Rotor design problem.

Meshes of 20 LFE elements were used to analyses the rotor for the two geometric variables in the range specified in Figure 16. The mass together with the elastic and plastic load factors were recorded and have been plotted as contours in Figure 17.

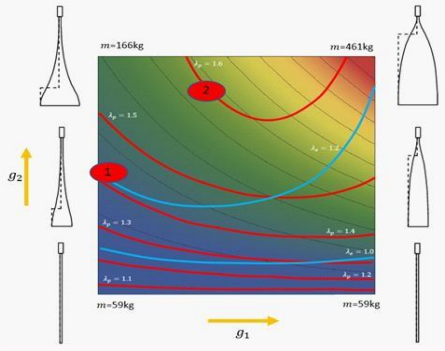

Figure 17: Rotor design solutions.

The filled color contours represent the mass of the rotor whilst the elastic load factor is shown as blue lines and the plastic load factor as red lines. Having constructed a graph of the form of that shown in Figure 17, the design engineer can very simply select designs of minimum mass for his/her particular choice of elastic and plastic load factors. Two design points are considered numbered 1 and 2 with red ellipses. From Eq. (17), and given that the design speed, ω_d, is 314rad/sec, the elastic and plastic limit speeds are for design point number 1 are 344 and 372 rad/sec respectively. For a yield stress, S_Y of 275MPa, the maximum equivalent stress at the design speed is also determined from the same equation as 229MPa. Similar calculations can be undertaken for design point

number 2 which has a larger plastic limit speed.

Discussion

It is common practice in industry to base the prediction of the burst speed on the average hoop stress from a linear-elastic analysis. The nature of rotating discs is that both the hoop and radial (principal) stresses are normally positive throughout the disc. It is also the case that for many disc geometries the hoop stress dominates the radial stress, i.e., $\sigma_h \geq \sigma_r$ for $r_i \leq r \leq r_o$. In these situations, a yield criterion such as the maximum principal stress criterion or the Tresca criterion will only involve the hoop stress and it is, therefore, seemingly reasonable to take the average elastic hoop stress as metric for the estimation of the plastic burst speed.

Early research involving the measurement of the plastic burst speed of rotating discs was undertaken by Robinson, [18]. Parallel-sided discs of a variety of materials were considered and the results are shown in Figure 18. In the burst criterion named after him, Robinson equated the average hoop stress to the material ultimate tensile strength (UTS) to determine the speed at which the disc was predicted to burst. The results illustrate that whilst this criterion might predict the upper limit for the burst speed, the majority of discs fail at a lower speed. If, however, the UTS is replaced with the yield stress then, with the exception of a single out-ridder, a seemingly reliable lower limit is obtained.

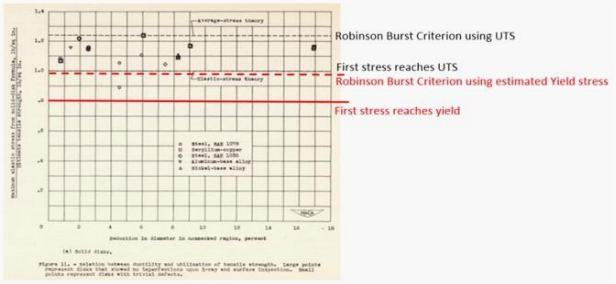

Figure 18: Measured results from NACA burst experiments [18].

Research undertaken later in provided the theoretical solution for the plastic burst speed of parallel-sided discs constrained by the Tresca yield criterion [13]. The theoretical solution agreed with the approach postulated by Robinson, i.e., that burst of a parallel-sided disc may be predicted using the average elastic hoop stress.

Clearly, using the average elastic hoop stress as a burst metric, whilst attractive in that a formal plastic analysis is not required, does have its limitations. Firstly, assuming that the von Mises yield criterion is a more suitable predictor of yield than Tresca and that the von Mises criteria circumscribes the maximum principal stress and Tresca criteria, adopting this approach will add a layer of conservatism to the burst prediction. Rather like neglecting the strengthening phenomenon of strain-hardening, this additional conservatism might be considered useful at the initial design stage. Secondly, there are disc geometries where the required dominance of the hoop stress does not hold. The disc used in Example 3 is one such case and in these circumstances, failure will be through radial rather than hoop burst.

Let us first consider the case of a conical disc which does have the required hoop stress dominance and confirm whether or not the equivalence between the prediction of plastic burst based on the average elastic hoop stress with that predicted using the Tresca yield criterion holds. The conical disc possesses a theoretical linear-elastic solution which is presented in [5]. Graphical results are presented for the displacements and stresses with a particular conical form. Although the LFE software has already been verified in the main body of this paper, c.f., Examples 1 & 2, software verification will first be undertaken on the example shown in section 6.63 (p127) of [5].

The thickness variation as a function of the radial ordinate, r, for a conical disc is given in Eq. (20) where the symbol t represents the axial thickness and the indexes i and o indicate the inner and outer radial positions respectively.

$$t = t_i + \frac{(t_o - t_i)}{r_o} r \qquad (20)$$

The theoretical linear-elastic solution for rotating conical discs is presented in chapter 6 of [5]. Figure 6.11 of that reference presents the solution in terms of stresses and displacement for the particular conical geometry shown in Figure 19.

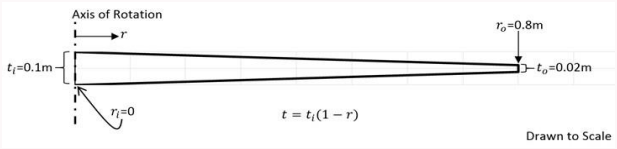

Figure 19: Conical disc example taken from section 6.63 (p127) of [5].

The material for the disc is assumed to be a steel with E=204GPa, ν=0.3 and ρ=7800kg/m^3. The results in [5] are presented for an angular velocity of ω=314 rad/s but only in graphical form. As such, a formal numerical verification cannot take place. Instead of this a graphical approach will be adopted whereby LFE results are superimposed on those presented in [5]. Such results are presented in Figure 20 for a meshes of 4 and 1024 LFE elements.

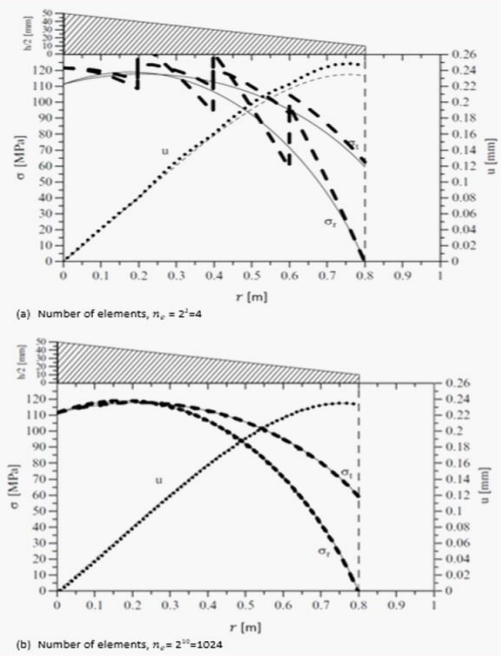

Figure 20: Elastic stresses from LFE overlaid on those of the analytical solution.

The agreement between the elastic stresses from the LFE model and the theoretical distributions shown for the refined 1024 element model is seen to be excellent as expected.

For the plastic analysis, a yield stress of S_y=500MPa was taken. The number of elements, n_e used in the mesh was $n_e = 2^m$ with $0 \leq m \leq 10$ and uniform mesh refinement was adopted. The convergence and yield plot for both conical and uniform thickness discs are shown in Figure 21.

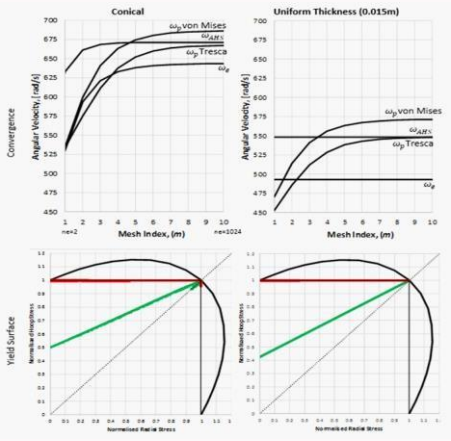

Figure 21: Convergence and yield for conical and uniform thickness discs.

Considering first the uniform thickness disc then the burst speed approximations based on the elastic analysis are, as expected, exact for the single element and do not change with mesh refinement. The plastic burst speeds based on the Tresca and von Mises criteria converge as expect from below the true solution with the result for the more conservative Tresca yield criteria below that for von Mises.

Richardson Extrapolation (RE), [19] is a commonly used method for determining an estimate of the exact value of a quantity of interest from a series of results obtained from successive refinements in a numerical method such as the FE method. It is often used in solution verification, [6]. The method is outlined in Eq. (21) for the quantity of interest φ. Three estimates of φ are required from successive meshes, i.e., φ_{m-2}, φ_{m-1} and φ_m to produce the estimate $\tilde{\varphi}_m$ The first step is to determine the rate of convergence, q, which is then used to predict the estimate as shown in the equation.

$$\tilde{\varphi}_m = \varphi_{m-1} - \frac{\varphi_{m-2} - \varphi_{m-1}}{2^q - 1}$$

$$q = \frac{\log\left[(\varphi_{m-2} - \varphi_{m-1})/(\varphi_{m-1} - \varphi_m)\right]}{\log(2)} \qquad (21)$$

The numerical results for the conical disc are shown together with the values from RE in Table 2.

	LFE Limit Speed Estimates, [rad/s]				RE for Plastic (Tresca)		RE for Plastic (AHS)	
m	Elastic	Plastic (Tresca)	AHS	Plastic (Mises)	Convergence Rate	Estimate, [rad/s]	Convergence Rate	Estimate, [rad/s]
0	492.7603	478.4744	548.1613	478.4744	\	\	\	\
1	530.3377	534.4208	632.9621	535.3081	\	\	\	\
2	593.8890	575.4733	661.1074	599.3490	0.4466	616.5258	1.5912	689.2526
3	621.3304	611.5506	668.7505	640.8733	0.1864	647.6279	1.8807	676.3936
4	633.3187	637.5323	670.7030	663.2901	0.4736	663.5140	1.9688	672.6556
5	638.6677	652.0070	671.1938	674.7940	0.8440	666.4817	1.9921	671.6847
6	641.2347	659.8208	671.3167	680.6551	0.8894	667.6347	1.9980	671.4396
7	642.4795	663.8724	671.3475	683.6064	0.9476	667.9239	1.9995	671.3782
8	643.0963	665.9373	671.3551	685.0872	0.9724	668.0022	1.9999	671.3628
9	643.4043	666.9797	671.3571	685.8289	0.9861	668.0222	1.9999	671.3590
10	643.5578	667.5036	671.3575	686.2001	0.9928	668.0274	2.0003	671.3580

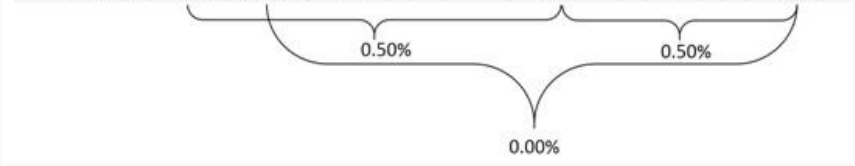

Table 2: Numerical results for conical disc.
As the mesh is refined, i.e., m increases the rates of convergence tend towards the theoretical values of q=1 and q=2 for the Plastic Tresca and AHS results respectively. The differences between the raw LFE results and the estimates of the exact values is small giving reassurance that the difference between the estimates for the Plastic Tresca and AHS results is realistically non-zero. It is noted that the estimate for AHS is greater than that for Plastic Tresca and can therefore be considered as unsafe.

It is seen that the rate of convergence tends towards one and two respectively for the plastic burst speed and for the AHS estimate of the burst speed. The estimates of the exact values obtained by RE enable an estimate of the error in the LFE quantities to be determined. It is seen that the error is about 0.5%. Using again the estimates of the exact values it is seen that there is a difference of 0.5% with the AHS value being greater than the plastic value using the Tresca criterion. This was indicated in the graphical results of Figure 21. For the uniform thickness disc, the results are presented in Table 3 where it is seen that the difference between these quantities is insignificant reinforcing the veracity of Robinson's burst criterion for uniform thickness discs.

	LFE Limit Speed Estimates, [rad/s]				RE for Plastic (Tresca)		RE for Plastic (AHS)	
m	Elastic	Plastic (Tresca)	AHS	Plastic (Mises)	Convergence Rate	Estimate, [rad/s]	Convergence Rate	Estimate, [rad/s]
0	492.7603	478.4744	548.1613	478.4744	\	\	\	\
1	492.7603	452.3081	548.1613	470.2005	\	\	\	\
2	492.7603	485.7575	548.1613	514.0281	*	*	*	*
3	492.7603	511.9462	548.1613	540.8617	0.3530	538.1349	*	*
4	492.7603	528.5258	548.1613	555.6224	0.6595	545.1053	*	*
5	492.7603	537.9169	548.1613	563.3185	0.8200	547.3080	*	*
6	492.7603	542.9260	548.1613	567.2612	0.9067	547.9352	*	*
7	492.7603	545.5146	548.1613	569.2553	0.9524	548.1031	*	*
8	492.7603	546.8306	548.1613	570.2579	0.9760	548.1466	*	*
9	492.7603	547.4941	548.1613	570.7606	0.9879	548.1577	*	*
10	492.7603	547.8273	548.1613	571.0123	0.9939	548.1604	*	*

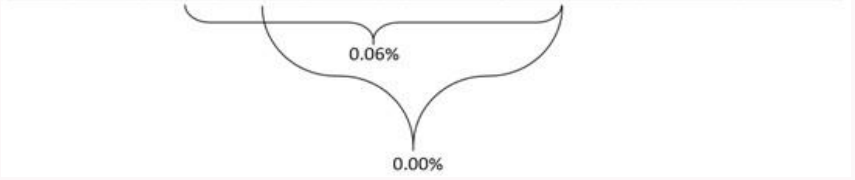

Table 3: Numerical results for uniform thickness disc.
As the mesh is refined the rate of convergence tend towards the theoretical unit value for the Plastic Tresca result. The LFE model provides exact values for AHS independent of the level of mesh refinement. It is noted also that the non-monotonic convergence seen for the first three meshes prevents the calculation of the RE estimate for the Plastic Tresca quantity of interest. In contrast to the conical disc, for this uniform thickness disc the difference between the estimates for the Plastic Tresca and AHS results is realistically zero and is in agreement with the result of [5].

This comparison provides a numerical example demonstrating that the Robinson criterion has restricted validity and that it can unsafely overpredict the correct plastic burst speed. Whilst the difference shown in this example, at 0.5%, is small in the overall scheme of engineering approximations, it would be interesting to consider at a future date whether this is always the case for discs of other geometries.

It was suggested earlier that there are two modes of failure for a rotating disc. These were identified as hoop burst and radial burst. The disc in Example 3 is of such a geometry that radial burst is the governing mode and this could have been predicted from the yield curves of Figure 15. This example has been reconsidered using now the Tresca yield criterion and a more refined mesh of 8 x 1024 = 8192 LFE elements. The results are presented in Figure 22 and Table 4.

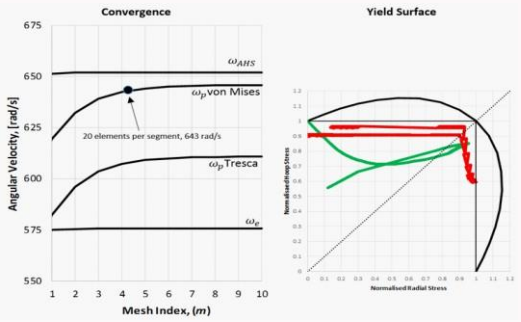

Figure 22: Convergence and yield for rotor of Example 3.
The yield curve of Figure 22 shows clearly that full yield is only developed at a single point. The difference between elastic and plastic curves also indicates significant stress redistribution has occurred during the plastic analysis.

	LFE Limit Speed Estimates, [rad/s]				RE for Plastic (Tresca)		RE for Plastic (AHS)	
m	Elastic	Plastic (Tresca)	AHS	Plastic (Mises)	Convergence Rate	Estimate, [rad/s]	Convergence Rate	Estimate, [rad/s]
0	559.3983	559.5212	649.4849	595.0680	\	\	\	\
1	574.8636	582.2870	651.3652	619.3179	\	\	\	\
2	575.4553	596.1185	651.8379	632.2584	0.7189	609.9500	1.9922	652.3105
3	575.6035	603.5662	651.9562	638.9621	0.8931	611.0139	1.9980	652.0745
4	575.6405	607.2275	651.9858	642.3438	1.0244	610.8888	1.9995	652.0154
5	575.6498	609.0251	651.9932	644.0367	1.0263	610.8227	1.9999	652.0006
6	575.6521	609.9165	651.9950	644.8829	1.0118	610.8080	2.0000	651.9969
7	575.6527	610.3605	651.9955	645.3058	1.0057	610.8045	1.9999	651.9959
8	575.6529	610.5826	651.9956	645.5172	0.9993	610.8047	2.0000	651.9957
9	575.6529	610.6935	651.9956	645.6229	1.0020	610.8044	2.0000	651.9956
10	575.6529	610.7489	651.9956	645.6757	1.0004	610.8043	1.9851	651.9956

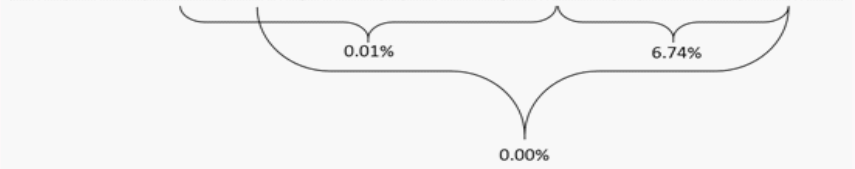

Table 4: Numerical results for disc of Example 3.
As the mesh is refined the rate of convergence tend towards the theoretical values for both the Plastic Tresca and AHS results. From the RE estimates of the exact values of the Plastic Tresca and AHS results it is seen that the LFE model is well converged. It should be noted here that whereas for other examples the mesh index, m, referred to the complete disc, for this model it refers to each of the eight segments. In the example, a mesh of 20 elements per segment was used which corresponds to a mesh index between 4 and 5. Taking the lower value, m=4, it is determined that the Plastic Tresca prediction of the burst speed is about 0.6% below the estimated exact value, i.e., well within the level of accuracy required in an engineering analysis.

The convergence plot in Figure 22 shows the burst speed prediction from the average elastic hoop stress but this is invalid since radial burst is the mode of failure for this disc. Convergence of the burst speed prediction made on the maximum elastic radial stress is presented in Figure 23. This quantity converges to a value significantly below the true plastic burst speed for the Tresca criterion (3.4%). The poor correlation between the prediction of burst based on the maximum elastic radial stress and the true plastic value is likely to be due to the significant stress redistribution noted earlier.

Predictions of the burst speed made from the results of an elastic analysis remain in use today for the initial design of rotating discs albeit with a generous safety factor presumably included to account for any uncertainty, see [20] for example. This might be considered surprising in that the theory of plasticity and FE systems capable of modelling plastic materials have long been available. It might be the case that plastic analysis has not been universally embraced because of lack of experience with plastic methods which are significantly more involved. The sort of experience required could be achieved by engineers having access to a design tool based on the LFE formulation and to use this to produce plastic solutions with which to compare with those generated from their preferred FE system.

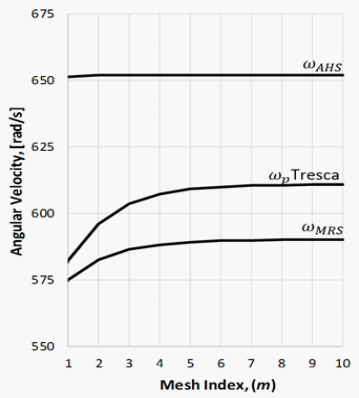

Figure 23: Convergence of elastic predictions of burst speed for disc of Example 3.

Conclusions & Further Work

The research presented in this paper extends the family of equilibrium finite elements (EFE) already available for safe structural design through plastic solutions that satisfy the lower-bound theorem of plasticity. Rather than approaching the formulation through the usual theoretical manner, a more direct approach has been used where the stiffness equations have been derived directly from the Lamé equations. In this way the element formulation might be better understood by practicing engineers who would normally be familiar with the Lamé equations but not necessarily so with FE theory. For this reason, the element has been called the Lamé Finite Element (LFE).

The LFE provides exact elastic solutions for rotating discs whose geometry is uniform of piecewise uniform thickness. For discs with smooth non-uniform geometry the piecewise uniform idealization offers a lower-bound solution which converges rapidly with mesh refinement. For plastic solutions the elastic compensation method (ECM) has been adopted which iteratively modifies the elastic modulus based on elastic analyses. Since, at the end of each iteration, the stresses are in strong equilibrium with the applied load, then provided the yield criterion is respected, the solution is a lower-bound to the exact solution.

These properties should make LFE models very attractive to the practicing engineer who might currently be using finite difference (FD) tools or those based on the conforming finite element (CFE) formulation. Neither FD and CFE methods possess the lower-bound property of LFE and for coarse meshes are likely to produce unsafe predictions of the burst speed. This imposes the requirement of undertaking solution verification on the practicing engineer and for most commercial systems this is a time-consuming manual process. In contrast, if the results from an unrefined LFE model are used then whilst a more economical use of material might be achieved through refining the LFE model, at least the result will be safe.

It is the case that uncertainty quantification is becoming more important in the reporting of numerical results. The use of dual analysis, where the disc is analyzed using both CFE and LFE models, can provide such uncertainty quantification for the burst speed. Whilst not offering a formal mathematical proof, through the work undertaken in the preparation of this paper it has been observed that the stiffness matrix for the LFE element is identical to that of the CFE element when reduced integration is used. This opens up the possibility of direct mapping between lower and upper-bound results through a simple post-processing operation and without the need to perform two analyses.

It is the case in industry that during the initial design of a disc, the burst speed is often predicted based on the elastic stress field. Whilst there are particular cases of disc geometry where this may be valid, it is easily demonstrated that this approach is generally invalid and can lead to the unsafe prediction of the plastic burst speed. It is suggested, therefore, that companies involved in the design of rotating discs might like to consider the adopting the LFE formulation presented in this paper in the software used for the design of discs.

References

1. Dominic Gates, Article in the Seattle Times, 4th November 2016
2. A.C.A. Ramsay, NAFEMS Benchmark Challenge Number 8, NAFEMS Benchmark Magazine **
3. Hearn EJ. Mechanics of materials 1: an introduction to the mechanics of elastic and plastic deformation of solids and structural materials. 3rd ed. Oxford: Butterworth-Heinemann; 1997.
4. Heyman J. Plastic Design of Rotating Discs. Proceedings of the Institution of Mechanical Engineers. 1958;172(1):531-547.

5. Vullo, Vincenzo & Vivio, Francesco, Rotors: Stress Analysis and Design, Springer-Verlag Italia 2013.
6. ASME.VV10 – Standard for verification and validation in computational solid mechanics; 2019.
7. Moitinho de Almeida, J.P. & Maunder, E.A.W., Equilibrium Finite Element Formulations, John Wiley & Sons Ltd, 2016.
8. Kaptan, A and Kisioglu, Y, Determination of burst pressures and failure locations of vehicle LPG cylinders, International Journal of Pressure Vessels and Piping, 84(7), 451-459 (July 2007).
9. Zienkiewicz, O. C. & Taylor, R. L., The Finite Element Method, Volume 2: Solid and Fluid Mechanics, Dynamics and Non-Linearity, McGraw-Hill, London, (1991).
10. Maunder EAW, Ramsay ACA. Equilibrium models for lower bound limit analyses of reinforced concrete slabs. ComputStruct. 2012;108–9:100–9.
11. Mackenzie D, Boyle JT, Hamilton R. The elastic compensation method for limit and shakedown analysis: a review. J Strain Anal Eng Des. 2000;35(3):171–88.
12. Taylor, G.I., Quinney, H., The Plastic Distortion of Metals, Philosophical Transactions of the Royal Society of London, Series A, Vol. 230, pp. 323-362, 1932.
13. Weiss, H.J., & Prager, W., The Bursting Speed of a Rotating Plastic Disc, Office of Naval Research, Technical Report Number 96, September, 1953.
14. Hearn EJ. Mechanics of materials 2: an introduction to the mechanics of elastic and plastic deformation of solids and structural materials. 3rd ed. Oxford: Butterworth-Heinemann; 1997.
15. Timoshenko, S.P., Strength of Materials, Part II, 3rd Edition, D. Van Nostrand Co., Princeton (NJ), 1956.
16. Grammel, R., DinglersPolytechnischen Journal, 338, p217, 1923.
17. Manson, S.S., Determination of Elastic Stresses in Gas-Turbine Disks, NACA Report 871, 1947.
18. Robinson, E., Bursting Tests of Steam-Turbine Disk Wheels, Trans. ASME 66, page 373, 1944.
19. Richardson LF, Gaunt JA. The deferred approach to the limit. Philos Trans R Soc A. 1927;226(636–46):299–349. doi: 10.1098/rsta.1927.0008
20. Robinson, C., Casey, M. and Woods I., An Integrated Approach to the Aero-Mechanical Optimisation of Turbo-Compressors, in Current Trends in Design and Computation of Turbomachinery, 2011.